1
Controlling fast chaos in opto-electronic delay dynamical systems

Lucas Illing, Daniel J. Gauthier, and Jonathan N. Blakely

1.1
Introduction

Recent studies have shown that fast chaotic dynamics can be used for a variety of applications such as information transmission with high power efficiency [1], generating truly random numbers [2,3], radar [4–8], as well as novel spread spectrum [9], ultrawide-bandwidth [10, 11], and optical [12, 13] communication schemes. In these applications, it is desirable to generate chaos in the fast regime where the typical time scale of the fluctuations is on the order of 1 ns or less [12, 14]. The ability to control the chaotic trajectory to specific regions in phase space is also desirable [1, 15, 16].

For applications requiring controlled trajectories, it is possible to use recently developed chaos-control methods. The key idea underlying these techniques is to stabilize a desired dynamical behavior by applying feedback through minute perturbations to an accessible parameter when the system is in a neighborhood of the desired trajectory in state-space [17–19].

In particular, many of the control protocols attempt to stabilize one of the unstable periodic orbits (UPOs) that are embedded in the chaotic attractor (although the control of unstable steady state has also been investigated, see, for example, Refs. [20–23]). Whereas the control of UPOs has been very successful for slow systems (characteristic time scale > 1 μs) [24–27], applying feedback control to fast chaotic systems is challenging because the controller requires a finite time to sense the current state of the system, determine the appropriate perturbation, and apply it to the system. This finite time interval, often called the control-loop latency τ_ℓ, can be problematic if the state of the system is no longer correlated with its measured state at the time when the perturbation is applied. Typically, chaos control fails when the latency is on the order of the period of the UPO to be stabilized [28–30].

Another difficulty faced in controlling fast chaos is the fact that many high-speed chaos generators are delay dynamical systems. Time-delayed feedback occurs naturally in high-speed systems, where the time it takes signals to propagate through the device components is comparable to the time scale of

Titel. Author(s)

ISBN: 3-527-XXXXX-X

the fluctuations. Hence many fast systems are most accurately described by time-delay differential equations. In fact, most fast chaos generators reported in the literature make explicit use of the propagation delay through components to generate delay-induced chaotic oscillations. Such systems evolve in an infinite dimensional phase space and can display very high-dimensional chaotic attractors [31]. Examples of fast broadband chaotic oscillators that are modeled as time-delay systems include electronic [32], opto-electronic [14,33], and microwave oscillators [1], as well as lasers with delayed optical feedback [12], and nonlinear optical resonators [34].

One approach to avoid the failure of chaos control due to latency is to simplify the controller as much as possible in order to minimize τ_ℓ. An example of this approach are methods that apply perturbations of a predetermined strength when the system crosses some threshold in phase space [35,36]. Using these methods, successful control of fast but low-dimensional chaos was demonstrated. As an example, an UPO with period $T_{PO} = 23$ ns was stabilized [35]. A drawback of these methods is that they rely on the ability to easily define windows and walls in phase space. This task is conceptually much more difficult in the case of delay systems where the phase space is infinite dimensional. Perhaps for this reason, these methods have not yet been applied successfully to delay systems.

The control of very fast chaotic delay dynamical systems is an outstanding problem because of two challenges that arise: control-loop latencies are unavoidable, and complex high-dimensional behavior of systems is common due to inherent time-delays. The primary purpose of this Chapter is to explain, by means of a simple example, why latency can be a significant problem adversely affecting control and to describe an approach for controlling time-delay systems even in the presence of substantial control-loop latency. This is a general approach that can be applied to any of the fast time-delay systems described above. As a specific example, we demonstrate this general approach by using time-delay autosynchronization control [37] to stabilize fast periodic oscillations ($T_{PO} \sim$12 ns) in an opto-electronic device. In principle, much faster oscillations can be controlled using, for example, high speed electronic or all-optical control components, paving the way to using controlled chaotic devices in high-bandwidth applications.

1.2 Control-loop latency: A simple example

To get an idea of why latency poses a practical problem, we consider in this section the control of a first-order linear dynamical system by a simple but commonly used control method known as proportional feedback [38]. In this

method, the controller produces a perturbation proportional to the difference between a measurement of the state of the system and a reference value. An analysis of this system provides a simple demonstration of how control fails due to latency.

Consider the linear differential equation

$$\dot{x} = ax \qquad \text{with} \quad a > 0 \tag{1.1}$$

and suppose it is our goal to stabilize the unstable fixed point x_* of this system, that is to stabilize $x_* = 0$.

Note that a is the exponential growth rate of perturbations and therefore a^{-1} is the natural time scale of the dynamical system. When control is added to the system, it is reasonable to expect that latency will degrade the performance of the controller when it is of the order of or greater than a^{-1}. In this case, the perturbation can grow significantly before the controller can respond. Before demonstrating this formally, let us examine the case of instantaneous feedback.

To apply proportional closed-loop feedback, the system's state is compared to a reference state (the fixed point in this case) and a signal proportional to the difference is fed back to the system affecting its future evolution. When the feedback is instantaneous, the dynamical system in the presence of the controller is described by the differential equation

$$\dot{x} = ax - \gamma(x - x_*) = (a - \gamma)x, \tag{1.2}$$

where γ denotes the strength of the feedback or control gain.

From Eq. (1.2), the effect of the controller is clear. If $\gamma > a$, the perturbation decays and the fixed point is stable. A useful method for visualizing the effect of a controller is to plot the control gain γ versus the parameter a, as is shown in Fig. 1.1(a). The region in this plot where the unstable state is stabilized by the controller is referred to as the domain of control.

The effect of latency on the controller can be quantified by determining how the domain of control changes as latency becomes significant. Suppose the control signal is applied at a time τ_ℓ later than it would be if it were instantaneous. The evolution of the dynamical system is then given by

$$\begin{aligned} \dot{x}(t) &= ax(t) - \gamma\{x(t - \tau_\ell) - x_*\}, \\ &= ax(t) - \gamma x(t - \tau_\ell). \end{aligned} \tag{1.3}$$

The controller's effect on the stability of the fixed point is determined by examining the evolution of a small perturbation $\delta = x - x_*$ of the form

$$\delta(t) = \delta_0 e^{\lambda t} \tag{1.4}$$

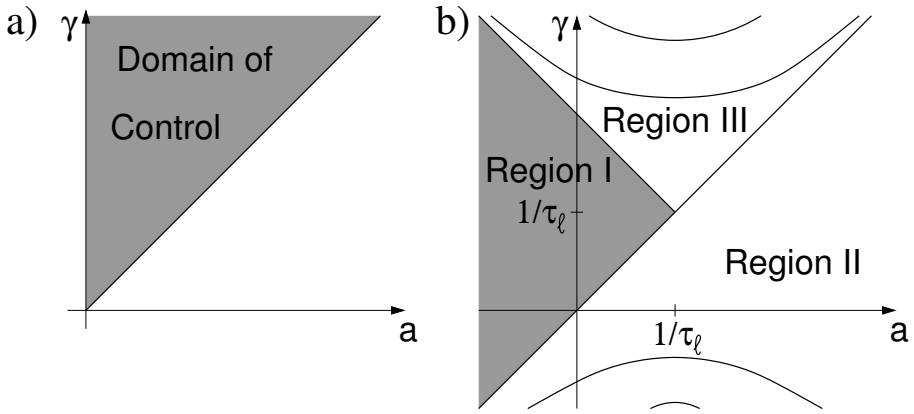

Fig. 1.1 Schematic depiction of the domain of control for the linear system with a) instantaneous control feedback [Eq. (1.2)] and with b) latency [Eq. (1.3)]

Substituting Eq. (1.4) into Eq. (1.3) yields the characteristic equation

$$\lambda - a + \gamma e^{-\lambda \tau_\ell} \quad = \quad 0. \tag{1.5}$$

The left hand side of Eq. (1.5) is known as the characteristic quasipolynomial and will be denoted $\Phi(\lambda)$. If the fixed point is stable, that is the perturbation decays, then $\Phi(\lambda)$ must have no roots with positive real parts. The region in the $a\gamma$ parameter space where this condition is satisfied is the domain of control.

Although the roots λ of Eq. (1.5) can be written in closed form in terms of the Lambert W function [39] in this simple example, it is instructive to determine the domain of control by the method of D-partition [40]. In this method, one divides the $a\gamma$ plane into distinct regions separated by curves on which $\Phi(\lambda)$ has at least one root with real part equal to zero. At all points within one such region of the plane, $\Phi(\lambda)$ has the same number of roots with a positive real part. To locate the domain of control, one has to identify the particular region in which that number is zero.

The first boundary is found by setting λ equal to zero to obtain the line

$$a = \gamma. \tag{1.6}$$

To obtain the rest, assume $\lambda = iy$ so that Eq. (1.5) becomes

$$iy - a + \gamma e^{-iy\tau_\ell} = 0. \tag{1.7}$$

Separating the real and imaginary parts gives the parametric form of the infinite set of curves that make up the remaining boundaries

$$a\tau_\ell = \frac{y\tau_\ell}{\sin(y\tau_\ell)} \cos(y\tau_\ell), \qquad \gamma\tau_\ell = \frac{y\tau_\ell}{\sin(y\tau_\ell)}. \tag{1.8}$$

One curve defined by these equations meets the line $a = \gamma$ at a cusp point $(a, \gamma) = (1/\tau_\ell, 1/\tau_\ell)$ and defines Region I, as is shown schematically in Fig. 1.1(b). The remaining infinte set of curves have an approximately hyperbolic shape and the curves' location is also indicated in Fig. 1.1(b).

In the case where $a < 0$ and no control is applied ($\gamma = 0$), the fixed point is stable so no solutions to Eq. (1.5) have positive real parts. Therefore, for all points in Region I of Fig. 1.1(b), there are no solutions to Eq. (1.5) with positive real parts. To determine the number of roots with positive real part in Region II, note that the characteristic equation reduces to the simple form

$$\lambda = a \tag{1.9}$$

along the line $\gamma = 0$, so there is clearly only one root with a positive real part.

To determine the number of roots with positive real part in Region III, consider the sign of the differential of the root of $\Phi(\lambda)$ with zero real part as a boundary is crossed. Specifically, if

$$\Phi(\lambda, a, \gamma) = 0, \tag{1.10}$$

then

$$\frac{\partial \Phi}{\partial \lambda} d\lambda + \frac{\partial \Phi}{\partial a} da + \frac{\partial \Phi}{\partial \gamma} d\gamma = 0. \tag{1.11}$$

The differential of the real part of the root is

$$\mathrm{Re}\,(d\lambda) = \mathrm{Re}\left(\frac{-\frac{\partial \Phi}{\partial a} da - \frac{\partial \Phi}{\partial \gamma} d\gamma}{\frac{\partial \Phi}{\partial \lambda}} \right). \tag{1.12}$$

Moving from Region II to III across the line $a = \gamma$, assuming $da < 0$, $d\gamma = 0$, and $\gamma > 1/\tau_\ell$, Eq. (1.12) becomes

$$\mathrm{Re}\,(d\lambda) = \frac{da}{1 - \gamma \tau_\ell} > 0. \tag{1.13}$$

The real part receives a positive increment, implying that points in Region III have at least one more root with positive real part than in Region II. A similar analysis of the other boundaries shows that further roots with positive real parts appear as each boundary is crossed on the line $a = 0$ moving away from Region I. Therefore, Region I is the only region with no unstable roots. The domain of control is simply the section of Region I to the right of the line $a = 0$ as shown in Fig. 1.1(b).

In contrast to the latency-free case, no control is possible when $\tau_\ell > a^{-1}$. Control can only be achieved if the latency is shorter than the characteristic

timescale of the system. This result is consistent with the intuitive argument presented above that perturbations to the system may grow too rapidly for the control response to be effective. Figure 1.1(b) also shows that the domain of control is of finite extent even when $\tau_\ell < a^{-1}$, whereas it extends to arbitrarily large values of feedback gain γ when latency is not present. Thus, large feedback gain tends to enhance the destabilizing effect of latency. Analogous effects of control loop latency have been found in chaos control schemes. Some examples are cited in the following section.

1.3 Controlling fast systems

Proportional feedback and related approaches have been very successful in controlling chaos in slow systems (characteristic time scale < 1 μs), but scaling these schemes to significantly higher frequencies, such as those encountered in high-speed electronic or optical systems, for example, is challenging for several reasons. One important issue in high-speed feedback control of chaotic systems is the latency through the control loop, as we have discussed in Sec. 1.2. An additional important issue is that it is difficult to accurately determine, store, and regenerate the reference state. The reference state in the example that is discussed in Sec. 1.2 is the fixed point $x_* = 0$. For the case where the stabilization of an UPO is the control aim, the reference state is the phase space trajectory of the UPO, denoted by $\mathbf{x}_*(t)$.

As first suggested by Pyragas [37], the UPOs of a dynamical system can be controlled using continuous feedback that does not require knowledge of $\mathbf{x}_*(t)$. In this scheme, which we refer to as 'time-delay auto-synchronization' (TDAS), the control perturbations are designed to synchronize the current state of the system to a time-delayed version of itself, with the time delay equal to one period of the desired orbit. Specifically, UPOs of period T_{PO} can be stabilized by continuous adjustment of an accessible parameter by an amount

$$\varepsilon(t) = -\gamma\,[s(t) - s(t-\tau)], \tag{1.14}$$

where τ is the delay with $\tau = T_{PO}$, γ is the control gain, and s is the measured signal, that is a function of the system's internal degrees of freedom. Note that $\varepsilon(t)$ vanishes when the system is on the UPO since $s(t) = s(t-\tau)$ for all t. This control scheme has been successfully applied to diverse experimental systems such as electronic circuits [28, 30, 41–43], Taylor-Couette fluid flow [44], an $^{15}NH_3$ laser [45], a strongly driven magnetic system [46], plasma instabilities [47, 48], and a chemical reaction [49, 50]; see also other chapters of this Handbook. The simplicity of TDAS allows it to be implemented with much less latency than most control schemes. However, some finite latency

is always present and, if large enough, can lead to failure as shown below. However, the main drawback to TDAS is that it is not effective at controlling highly unstable orbits.

Socolar *et al.* [51] introduced a generalization of TDAS, called 'extended time-delay auto-synchronization' (ETDAS), that is capable of extending the domain of effective control significantly [30, 52] and is easy to implement in high-speed systems. Stabilizing UPOs is achieved by feedback of an error signal that is proportional to the difference between the value of a state variable and an infinite series of values of the state variable delayed in time by integral multiples of τ. Specifically, ETDAS prescribes the continuous adjustment of the system parameter by

$$\varepsilon(t) = -\gamma\,[s(t) - (1-R)\sum_{k=1}^{\infty} R^{k-1} s(t-k\tau)], \tag{1.15}$$

where -1$\leq R < 1$ regulates the weight of information from the past. Highly unstable orbits can be stabilized as $R \to 1$. The case $R = 0$ corresponds to TDAS. We emphasize that, for any R, $\varepsilon(t)$ vanishes when the UPO is stabilized since $s(t-k\tau) = s(t)$ for all t and k, so there is no power dissipated in the feedback loop whenever ETDAS is successful. Note that no property of the UPO must be known in advance except its period. In periodically driven systems, where the period of the orbit is determined from the driving, no features of the UPO need ever be determined explicitly. The control parameters γ and R can be determined empirically in an experiment or by performing a linear stability analysis of the system in the presence of ETDAS feedback control [53, 54].

TDAS and ETDAS are often the control method of choice in high-speed chaotic systems because they are continuous feedback controllers that do not require knowledge of a reference state. Nevertheless, deleterious effects of control loop latency have also been found in these chaos control schemes. For example, Sukow *et al.* [30] investigated the effect of latency on control of a fast chaotic electronic circuit using ETDAS. The electronic circuit was a diode resonator and is shown schematically in Fig. 1.2(a). In both cases, the domain of control decreased in size as the latency increases, until control is finally lost.

As can be seen in Figure 1.2(b), the maximum latency at which control was attained was as much as four times larger with ETDAS than TDAS, but ETDAS control failed when the latency reached $\sim$ 86% of the correlation time of the uncontrolled orbit even in the best case observed. Just *et al.* [28] developed an approximate prediction for the critical latency at which TDAS control fails. They predict TDAS control can be achieved when

$$\tau_\ell < T_{PO}\frac{(1-\nu T_{PO}/2)}{\nu T_{PO}}, \tag{1.16}$$

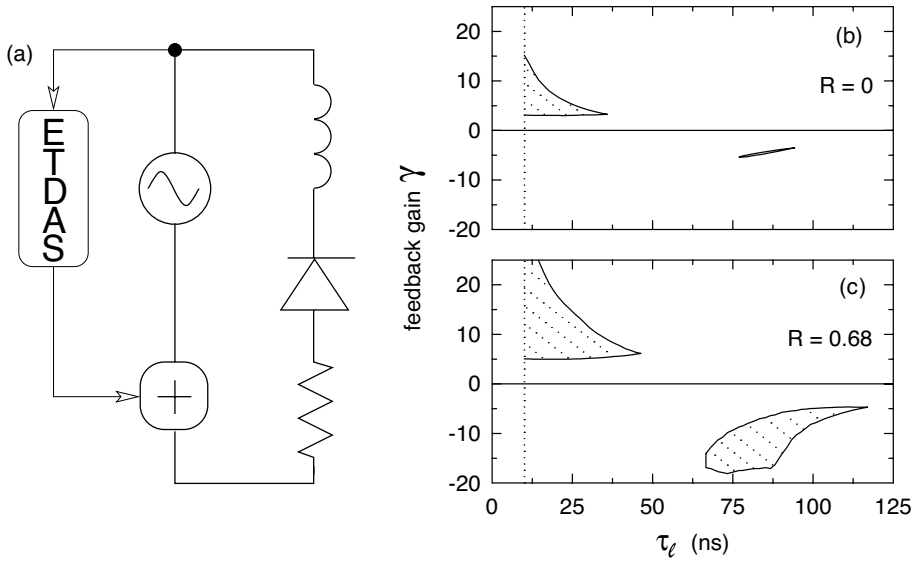

Fig. 1.2 Diode Resonator. a) Schematic of circuit: It consists of a rectifier diode, an inductor and a resistor, which is driven by a leveled sinusoidal voltage (10.1 MHz) that passes through a high-speed signal conditioner where it is combined with the controller signal. b) Effects of control-loop latency τ_ℓ on the domain of control for the period-1 UPO. Controlled regions are shown for R=0 and R=0.68. The dashed vertical line at $\tau_\ell = 10$ ns indicates the minimum latency attainable with our implementation of ETDAS.

where T_{PO} and ν are the period and Floquet exponent (or average growth rate of perturbations) of a the UPO to be stabilized, respectively. This prediction was tested in experiments on a nonlinear electronic circuit with Rössler type behavior. Control failed experimentally when the latency reached a value $\sim$ 11% of the period of the UPO. Equation (1.16) predicted failure at $\sim$ 12.5% of the period, in reasonable agreement with the experiemental results [28].

We have discovered that the effects of control-loop latency can be mitigated when controlling chaotic systems involving a nonlinear element and an inherent time-delay T_D, as shown schematically in Fig. 1.3a. Chaos can be controlled in time-delay systems by taking advantage of the fact that it is often possible to measure the state of the system at one point in the time-delay loop (p_1) and to apply perturbations at a different point (p_2), as shown in Fig. 1.3b. Such distributed feedback is effective because the state of the system at p_2 is just equal to its state p_1 delayed by the propagation time $T_D - \tau_{21}$ through the loop between the points. The arrival of the control perturbations at p_2 is timed correctly if

$$\tau_\ell + \tau_{21} = T_D. \tag{1.17}$$

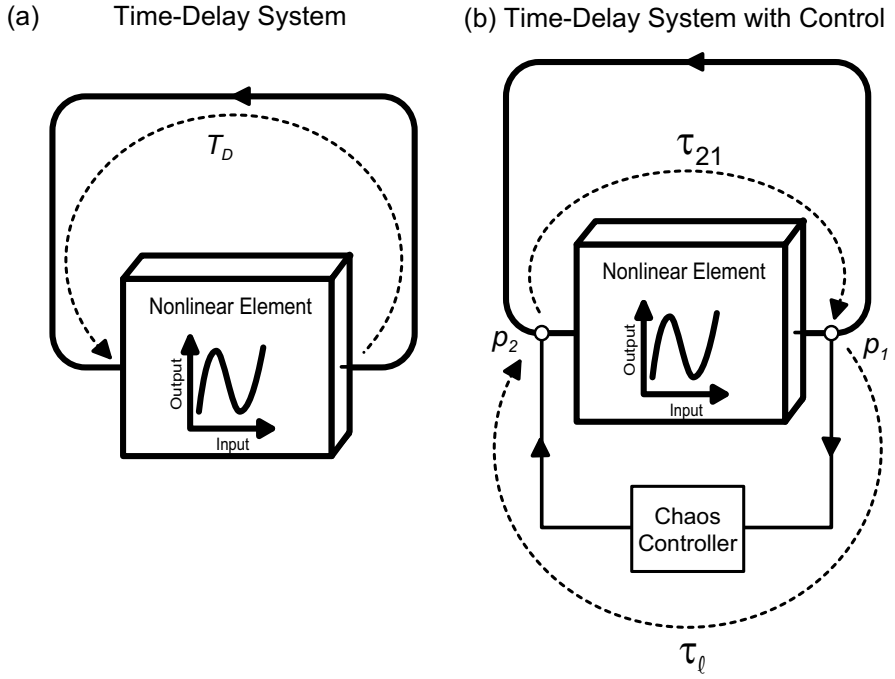

Fig. 1.3 (a) Schematic of a typical topology of a time-delay system consisting of a nonlinear element and a long loop connecting the output to the input of the element, introducing a total time-delay T_D. (b) Schematic of feedback control that measures the state at point p_1 and perturbs the system at p_2. The propagation time through the controller (control loop latency) is denoted by τ_ℓ and τ_{21} is the propagation time from p_2 to p_1. Note that the signal takes a time $T_D - \tau_{21}$ to get from p_1 to p_2.

Hence, it is possible to compensate for a reasonable amount of control loop latency τ_ℓ by appropriate choice of p_1 and p_2. The advantage of this approach is that the propagation time through the controller does not have to be faster than the controlled dynamics. In contrast, the conventional approach for controlling chaos is to perform the measurement and apply the perturbations instantaneously ($\tau_\ell \to 0$), which requires controller components that are much faster than the components of the chaotic device to approximate instantaneous feedback. Note that we have not specified a method of computing the control perturbations. In principle, any of the existing methods [18] may be used as long as they can be implemented with latency satisfying Eq. (1.17).

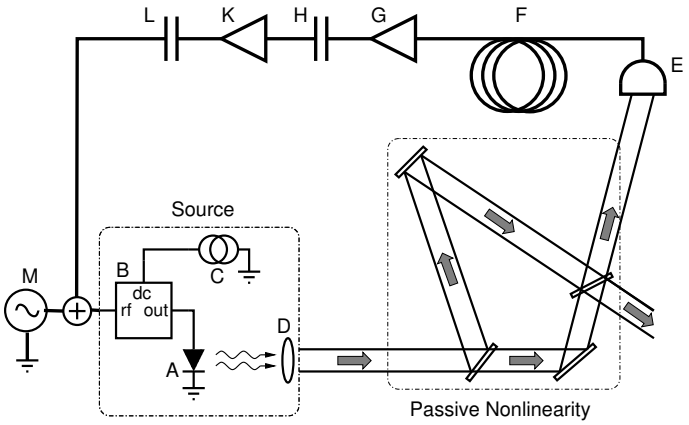

Fig. 1.4 Experimental setup of a chaotic time-delay device of the type shown in Fig. 1.3(a). The device consists of a voltage controlled source, a passive nonlinearity, and a feedback loop with bandpass characteristics. The components labeled A-M and details of the setup are explained in the text.

1.4 A fast opto-electronic chaos generator

To demonstrate the feasibility of controlling fast chaos using this general concept, we apply it to a chaotic opto-electronic device. The device consists of the laser, which acts as a current-controlled source, the interferometer, which constitutes the passive nonlinearity in the system, and the feedback loop with bandpass characteristics. A schematic of the experimental setup is shown in Fig. 1.4, where the labels A-M correspond to components that we refer to and describe below.

The light source is an AlGaInP diode laser (A - Hitachi HL6501MG, wavelength 0.65 μm) with a multi-quantum well structure. The diode is housed in a commercial mount (B - Thorlabs TCLDM9) equipped with a bias-T for adding an RF component to the injection current. Thermoelectric coolers in the mount are connected to a proportional-integral-derivative feedback controller (Thorlabs TEC2000) to provide 1 mK temperature stability thereby minimizing frequency and power drift. The output light of the laser is collimated by a lens (D - Thorlabs C230TM-B, f=4.5 mm) producing an elliptical beam (1 mm $\times$ 5 mm) with a maximum output power of 35 mW.

The passive nonlinearity in the experiment consists of a Mach-Zehnder interferometer with unequal path lengths (path difference 45 cm) into which the laser beam is directed. A silicon photodetector (E - Hammamatsu S4751, DC-750 MHz bandwidth, 15 V reverse bias) measures the intensity of light emitted from one output port of the interferometer. The size of the photodiode is much smaller than the width of the laser beam so only a fraction of

the interferometer's output is detected. The small detector size ensures that only one fringe appears within the beam cross section thus compensating for wavefront aberrations and slight laser beam misalignment and improving the fringe visibility. A neutral density filter is fixed to the front of the laser mount limiting the optical power reaching the photodiode to prevent saturation.

The feedback-loop photodiode produces a current proportional to the optical power falling on its surface. The current flows through a 50 Ω resistor. The voltage across that resistor is transmitted down a coaxial cable (F - RU 58, total length $\sim$ 327 cm). The signal emanating from the cable passes through a low-noise, fixed-gain, AC-coupled amplifier (G - MiniCircuits ZFL-1000LN, bandwidth 0.1-1000 MHz), a DC-blocking chip capacitor (H - 220 pF), an AC-coupled amplifier (K - Mini-Circuits ZFL-1000GH, bandwidth 10-1200 MHz), and a second DC-blocking chip capacitor (L - 470 pF). The capacitors reduce the loop gain at frequencies below $\sim$ 7 MHz, where a thermal effect enhances the laser's sensitivity to frequency modulation [55, 56]. The system is subject to an external driving force provided by adding an RF voltage to the feedback signal (M). (The driven system has more prominent bifurcations than the undriven device.) The resulting voltage is applied to the bias-T (B) in the laser mount. The bias-T converts the signal into a current and adds it to a DC injection current from a commercial laser driver (C - Thorlabs LDC500). The length of the coaxial cable can be adjusted to obtain values of the time-delay T_D in the range 11 - 20 ns.

This opto-electronic device displays a range of periodic, quasiperiodic, and chaotic behavior [57] that is set by the amplifier gain and the ratio of the time-delay to the characteristic response time of the system (typically set to a large value). As an example, we show, in Figure 1.5, experimental time series and power spectra of the optical power at the second interferometer port with $V_m = 225$ mV and $\Omega_m/2\pi = 51.7$ MHz. With the feedback gain below $\Gamma = 6.7 \pm 0.4$ mV/mW, the system displays a periodic oscillation at the external modulation frequency (to within the 300 kHz resolution bandwidth of the spectrum analyzer) as shown in Fig. 1.5(a,c). As the gain increases, a peak appears in the power spectrum at about half the fundamental frequency. As the gain is increased further, the broad background rises and the tall peaks at the fundamental frequency and its harmonics weaken. The power spectrum for $\Gamma = 15.0 \pm 0.5$ mV/mW, shown in Fig. 1.5(d), is quite broad and the peaks have nearly dropped to the level of background which has risen significantly above the noise floor. This is indicative of high-dimensional chaos in the system.

A theoretical model for the opto-electronic device is given by [57]

$$\tau_l \dot{V}(t) = -V(t) + \Gamma P(t - T_D)\ \{1 + b \sin[\alpha\,(P(t - T_D) - P_0)]\}\,, \quad (1.18)$$

$$\dot{P}(t) = -\frac{1}{\tau_h}\,(P(t) - P_0) + \kappa\left[\dot{V}(t) + \Omega_m V_m \cos(\Omega_m t)\right]. \quad (1.19)$$

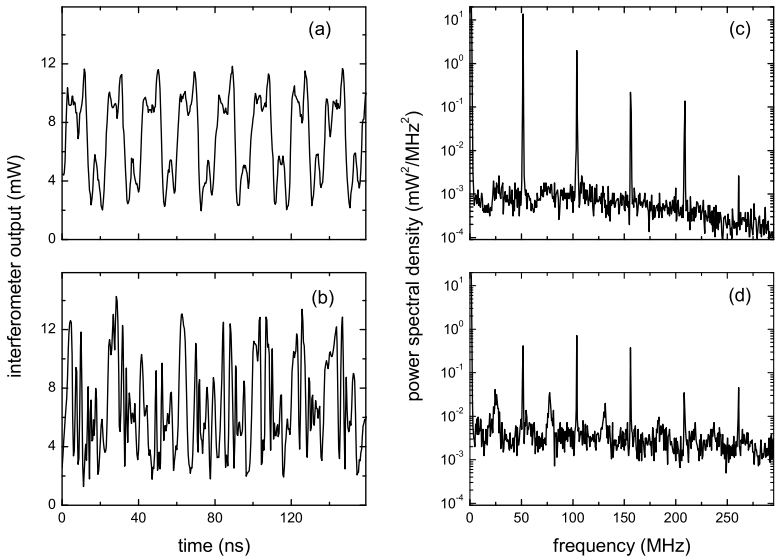

Fig. 1.5 Experimentally measured time series and power spectra of the output power at the second port of the active interferometer with external modulation showing route to chaos as Γ is increased. The loop gain Γ is (a,c) 2.2 mV/mW and (b,d) 15.4 mV/mW.

All parameters in this model can be measured and are displayed in Tab.1.1.

Using the same gain values as in the experiment, very similar time series and power spectra are produced by the model, as shown in Fig. 1.6. With $\Gamma = 2.2$ mV/mW, as shown in Fig. 1.5(a), the model displays a period one orbit. In Fig. 1.6(d), where $\Gamma = 15.4$ mV/mW, the power spectrum is considerably flattened and the system is clearly chaotic. High dimensional chaos is also confirmed in numeric simulations that determine the Lyapunov spectrum and find positive Lyapunov exponents and attractor Lyapunov dimension $D_L \gg 5$ [57].

1.5 Controlling the fast opto-electronic device

We apply our control method to the opto-electronic device using the setup shown in Fig. 1.7 by measuring the state of the system (denoted by $s(t)$) at point p_1 and injecting continuously a control signal $\varepsilon(t + \tau_\ell)$ at point p_2. For a given device time-delay T_D, coaxial cable can be added or removed from the control loop to obtain a value of $\tau_\ell + \tau_{21}$ satisfying Eq. (1.17). To compute the control perturbations ε, we use TDAS, that is the controller synchronizes the system to its state one orbital period in the past by setting $\varepsilon(t) = -\gamma[s(t) -$

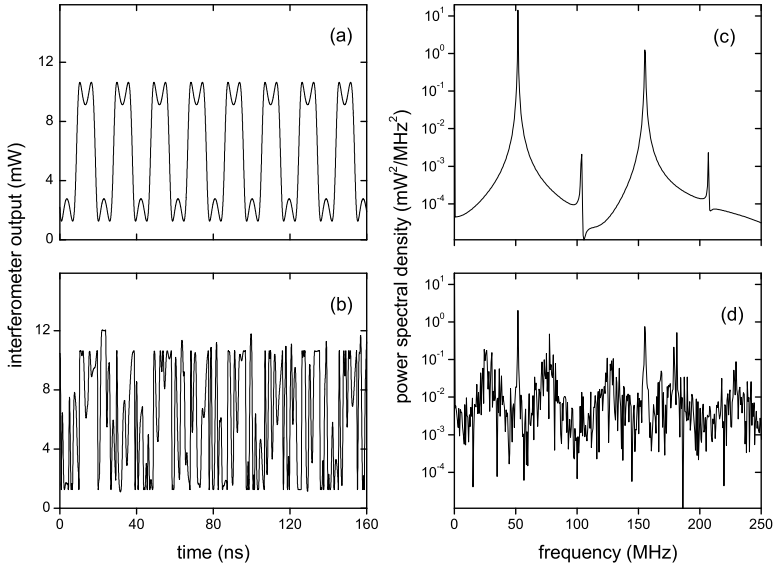

Fig. 1.6 Time series and power spectra from the numerically integrated model of the modulated system showing the route to chaos. The gain Γ is (a, c) 2.2 mV/mW and (b, d) 15.4 mV/mW.

Tab. 1.1 Definition of symbols and measured values of the model parameters.

Symbol	Value	Description
τ_l	0.66 ± 0.05 ns	Low-pass filter time constant
τ_h	22 ± 0.5 ns	High-pass filter time constant
T_D	19.1 ± 0.1 ns	Device delay-time
κ	$(4.8 \pm 0.1)\ \mu$W/mV	Modulation sensitivity
α	1.89 ± 0.05 mW^{-1}	Interferometer sensitivity
b	0.8 ± 0.02	Fringe visibility
P_0	26 ± 0.5 mW	Operating point optical power
Γ	0 - 18 mV/mW	Feedback gain
V_m	225 mV	External drive amplitude
Ω_m	3.25 10^8 rad/s	External drive frequency

$s(t-\tau)]$ where τ is a control-loop delay that is set equal to the period T_{PO} of the desired orbit, and γ is the control gain [37, 42]. When synchronization with the delayed state is successful, the trajectory of the controlled system is precisely on the UPO and the control signal is comparable to the noise level in the system. We emphasize that this modified TDAS control was chosen for ease of implementation in this proof-of-concept experiment but that our

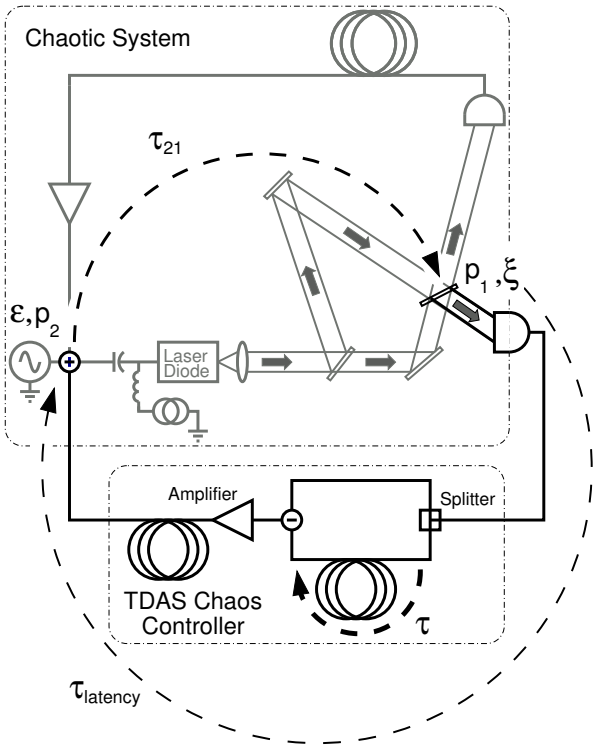

Fig. 1.7 Experimental system with controller. The measurement point p_1 is the second beam splitter of the interferometer. Perturbations are applied at p_2, an RF-power combiner. The time τ_{21} for a signal to propagate from point p_2 to p_1 is $\sim$ 3 ns. The controller contains two delay lines, the first sets τ, the period of the orbit to be controlled, the second is used to adjust the latency τ_ℓ to properly time the arrival of perturbations at p_2. The state of the system is monitored through a directional coupler positioned directly after the photodiode in the delay loop of the opto-electronic device. The control signal is measured through a directional coupler at the output of the controller.

approach is consistent with other control methods applicable to delay systems (for example [51, 58]).

Controlling the fast opto-electronic device is initiated by setting the various control-loop time delays ($\tau_\ell + \tau_{21}$ and τ) and applying the output of the TDAS controller to point p_2 with γ set to a low value ($\gamma = 0.1$ mV/mW). Upon increasing γ to 10.3 mV/mW, we observe that $\varepsilon(t)$ decreases, which we further minimize by making fine adjustments to τ and $\tau_\ell + \tau_{21}$. Successful control is indicated when $\varepsilon(t)$ drops to the noise level of the device. Figure 1.8(c) shows the periodic temporal evolution of the controlled orbit with a period of $T_{PO} \sim$12 ns. The corresponding power spectrum, shown in Fig. 1.8(d), is dominated by a single fundamental frequency of 81 MHz and its harmonics. The

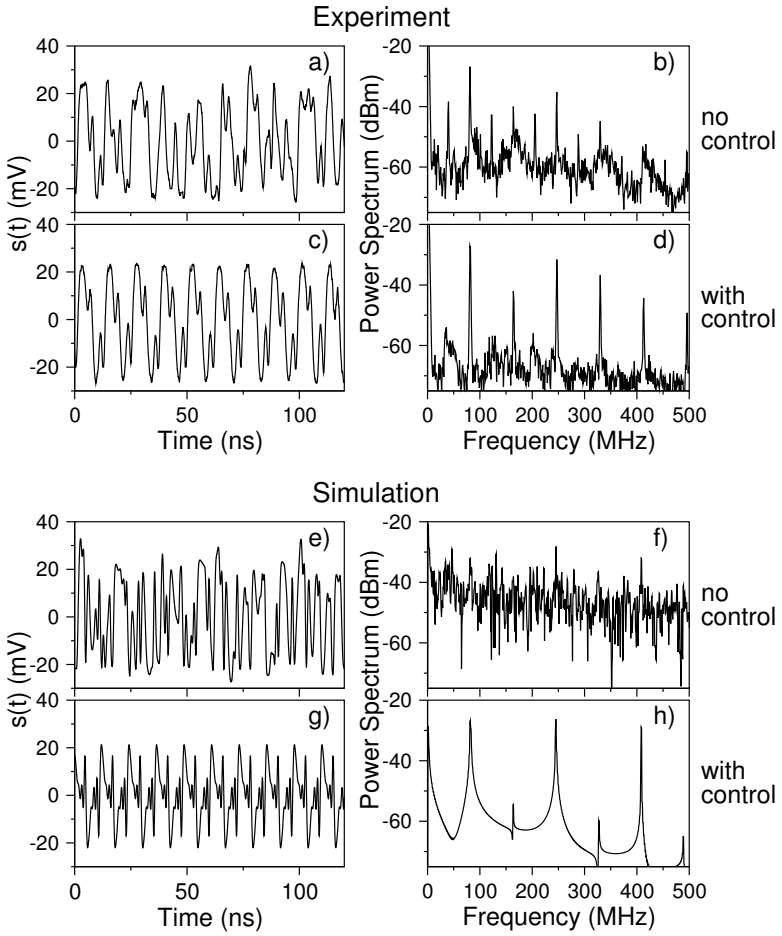

Fig. 1.8 Experimental (a-d) and simulated (e-h) data showing control of fast chaos. The state of the system is monitored by measuring the voltage in the delay loop before the amplifier (see Fig. 1.7). The device delay-time is $T_D \sim 11$ ns. (a) The chaotic time series of the monitored voltage in the absence of control, (b) the corresponding broad power spectrum, (c) the periodic time series of the stabilized orbit with control on, and (d) the corresponding power spectrum. The effect of control in simulations is consistent with our experimental results, as shown by the simulated time series of the monitor voltage without (e) and with (g) control and the corresponding power spectra (f) and (h).

observation of successful stabilization of one of the UPOs embedded in the chaos of the uncontrolled opto-electronic device is consistent with the theoretical prediction of a mathematical model describing the opto-electronic device in the presence of control, as shown in Figs. 1.8(g,h), where the simulated time series and power spectrum, respectively, indicate periodic oscillations.

The data shown in Fig. 1.8 are the primary result of this experiment, demonstrating the feasibility of controlling chaos in high-bandwidth systems even

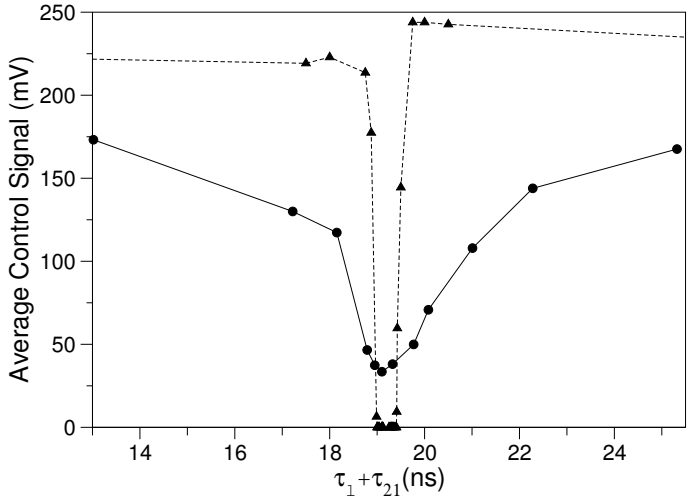

Fig. 1.9 Time-averaged control signal in the experiment (circles) and simulation (triangles). The minimum centered around $T_D = 19.1$ ns is the region of successful control, where $\langle \varepsilon(t) \rangle$ is at the noise level ($\sim$ 30 mV, estimated by breaking the control loop and measuring the control signal when the opto-electronic device is in a periodic regime). The width of the minimum ($\sim$ 0.5 ns) indicates that control succeeds despite small errors in $\tau_\ell + \tau_{21}$. Noise in the experiment smooths out the sharp transition from controlled to uncontrolled behavior observed in simulation.

when the latency is comparable to the characteristic time scales of the chaotic device (compare $T_{PO} \sim$12 ns and $\tau_\ell \sim 8$ ns).

To control this fast UPO, we used the smallest value of $\tau_\ell + \tau_{21}$ attainable with our current experimental apparatus. Hence, it is not possible to fully explore the effects on control when we change τ_{21}. Therefore, we slowed down the chaotic opto-electronic device by increasing the device delay-time T_D. In this way, we can explore $(\tau_\ell + \tau_{21})$ over a range including values that are shorter than T_D. Figure 1.9 shows the size of the measured (circles) and predicted (line) control perturbations as a function of $\tau_\ell + \tau_{21}$. It is seen that control is possible over a reasonably large range of time delays ($\sim$0.5 ns) centered on T_D so that it is not necessary to set precisely the control-loop delay, a practical benefit of this scheme.

From the data shown in Fig. 1.9, we can infer what would happen if $p_1 = p_2$ (the conventional method of implementing chaos control with nearly instantaneous feedback). In this case, $\tau_{21} = T_D$ and hence control would only be effective when $\tau_\ell <$0.5 ns, which is not possible using our implementation of TDAS.

Increasing the feedback gain Γ of the chaotic opto-electronic device increases the complexity of the dynamics, that is the dimension of the chaotic attractor grows [31,57]. In Fig. 1.10 we show that the domain of control shrinks

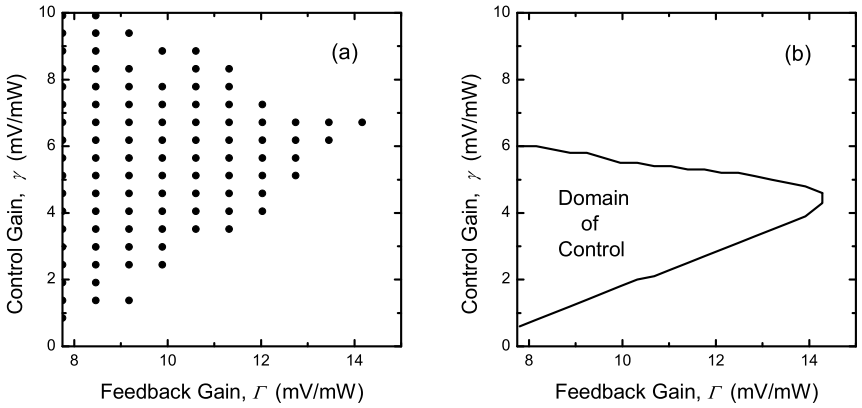

Fig. 1.10 (a) Experimental and (b) theoretical domains of control in the parameter plane spanned by feedback gain Γ of the chaotic opto-electronic device and the control gain γ. The device delay-time was $T_D = 19.1$ ns.

Chaos Control Method	**Orbit Period,** T_{PO}	**Control Loop Latency,** τ_ℓ
TDAS [30, 51]	99 ns	$<$30 ns
ETDAS [30, 51]	99 ns	$<$120 ns
Pulsewidth Modulation [35]	52 ns	4.4 ns
Limiter Control [36]	23 ns	$\lesssim$ 1 ns [1]
Modified TDAS [59]	12 ns	8 ns

Tab. 1.2 Period of some experimentally stabilized UPOs and latency of the controller. The modified TDAS method described in this chapter is used to stabilize the UPO with the highest frequency reported to date. Note that with this method the latency need not be small compared to the period of the orbit. [1)N. Corron, private communication]

as Γ is increased and that control fails for large values of Γ ($\Gamma > 14$ mV/mW). This demonstrates that the modified TDAS control fails to stabilize UPOs when the opto-electronic device operates in a regime of high-dimensional chaos in the absence of control. The domain of control could be increased by using ETDAS. However, experimental implementation of ETDAS is likely to be more challenging than the modified TDAS method because, in many cases, it can require a predistortion stage in the controller [30]. Thus, the modified TDAS method provides a balance of design simplicity and tolerance to latency.

1.6 Outlook

In this chapter, we have demonstrated control of a fast delay dynamical system using a controller with substantial control-loop latency. For comparison, we list in Table 1.2 the period of the stabilized UPO and the estimated controller latency for a few experiments that have been reported in the literature. Note that the modified TDAS controller discussed in this paper not only controls fast systems, that is, stabilizes the UPO with the shortest period, but that the latency of the modified TDAS controller is nearly equal to the period of the stabilized orbit. This tolerance to latency is in contradistinction to other methods such as limiter control but is shared by ETDAS, which also has demonstrated a similar tolerance to latency.

In principle, faster time-delay chaotic systems can be controlled using our approach as long as the controller uses technology (for example, integrated circuits, all-optical) that is as fast as the system to be controlled so that τ_ℓ is comparable to T_D. Traditional chaos control schemes require that τ_ℓ be much shorter than T_D, increasing substantially the cost and complexity of the controller. With regards to potential applications, we note that adjustments to our controller allows for controlling different UPOs embedded in the chaotic system, which could be used for symbolic-dynamic-based communication schemes. Overall, our research points out the importance of using time-delay dynamical systems combined with distributed control for applications requiring fast controlled chaos.

Finally, our approach of control in the presence of control-loop latency is equally useful for non-chaotic fast and ultrafast time-delay devices, where the fast time scale makes the suppression of undesired instabilities challenging (for example the double pulsing instability in femtosecond fiber lasers [60].)

References

1 V. Dronov, M. Hendrey, T. Antonsen, and E. Ott, "Communication with a chaotic traveling wave tube microwave generator," Chaos **14**, 30 (2004).

2 J. Gleeson, "Truly random number generator based on turbulent electroconvection," Appl. Phys. Lett. **81**, 1949 (2002).

3 T. Stojanovski, J. Pihl, and L. Kocarev, "Chaos-based random number generators - part ii: Practical realization," IEEE Trans. Circuits Syst. I, Fundam. Theory Appl. **48**, 382 (2001).

4 F. Y. Lin and J. M. Liu, "Ambiguity functions of laser-based chaotic radar," IEEE J. Quantum Electron. **40**, 1732 (2004).

5 B. C. Flores, E. A. Solis, , and G. Thomas, "Assessment of chaos-based fm signals for range-doppler imaging," IEE Proc.-Radar Sonar Navig. **150**, 313 (2003).

6 V. Venkatasubramanian and H. Leung, "A novel chaos-based high-resolution imaging technique and its application to through-the-wall imaging," IEEE Signal Processing Lett. **12**, 528 (2005).

7 K. Myneni, T. A. Barr, B. R. Reed, S. D. Pethel, and N. J. Corron, "High-precision

ranging using a chaotic laser pulse train," Appl. Phys. Lett. **78**, 1496 (2001).

8 T. Carroll, "Chaotic system for self-synchronizing doppler measurement," Chaos **15**, 013109 (2005).

9 M. Kennedy, G. Kolumban, G. Kis, and Z. Jako, "Performance evaluation of fm-dcsk modulation in multipath environments," IEEE Trans. Circuits Syst. I, Fundam. Theory Appl. **47**, 1702 (2000).

10 N. F. Rulkov, M. M. Sushchik, L. S. Tsimring, and A. R. Volkovskii, "Digital communication using chaotic-pulse-position modulation," IEEE Trans. Circuits Syst. I, Fundam. Theory Appl. **48**, 1436 (2001).

11 G. M. Maggio, N. Rulkov, and L. Reggiani, "Pseudo-chaotic time hopping for uwb impulse radio," IEEE Trans. Circuits Syst. I, Fundam. Theory Appl. **48**, 1424 (2001).

12 G. VanWiggeren and R. Roy, "Communication with chaotic lasers," Science **279**, 1198 (1998).

13 A. Argyris, D. Syvridis, L. Larger, V. Annovazzi-Lodi, P. Colet, I. Fischer, J. García-Ojalvo, C. R. Mirasso, L. Pesquera, and K. A. Shore, "Chaos-based communications at high bit rates using commercial fibre-optic links," Nature **437**, 343 (2005).

14 H. D. I. Abarbanel, M. B. Kennel, L. Illing, S. Tang, H. F. Chen, and J. M. Liu, "Synchronization and communication using semiconductor lasers with optoelectronic feedback," IEEE J. Quantum Electron. **37**, 1301 (2001).

15 S. Hayes, C. Grebogi, and E. Ott, "Communication with chaos," Phys. Rev. Lett. **70**, 3031 (1993).

16 H. D. I. Abarbanel and P. S. Linsay, "Secure communications and unstable periodic orbits of strange attractors," IEEE Trans. Circuits Syst. II **40**, 643 (1993).

17 E. Ott, C. Grebogi, and J. A. Yorke, "Controlling chaos," Phys. Rev. Lett. **64**, 1196 (1990).

18 D. J. Gauthier, "Resource letter: CC-1: Controlling chaos," Am. J. Phys. **71**, 750 (2003).

19 L. Illing, D. J. Gauthier, and R. Roy, *Controlling Optical Chaos, Spatio-Temporal Dynamics, and Patterns* (Academic Press, 2006), vol. 54 of *Advances In Atomic, Molecular, and Optical Physics*.

20 A. Chang, J. Bienfang, G. Hall, J. Gardner, and D. Gauthier, "Stabilizing unstable steady states using extended time-delay autosynchronization," Chaos **8**, 782 (1998).

21 D. Gauthier, "Controlling lasers by use of extended time-delay autosynchronization," Opt. Lett. **23**, 703 (1998).

22 A. Ahlborn and U. Parlitz, "Stabilizing unstable steady states using multiple delay feedback control," Phys. Rev. Lett. **93**, 264101 (2004).

23 S. Yanchuk, M. Wolfrum, P. Hövel, and E. Schöll, "Control of unstable steady states by long delay feedback," Phys. Rev. E **74**, 026201 (2006).

24 R. Roy, T. W. Murphy, Jr., T. D. Maier, Z. Gills, and E. R. Hunt, "Dynamical control of a chaotic laser: experimental stabilization of a globally coupled system," Phys. Rev. Lett. **68**, 1259 (1992).

25 E. R. Hunt, "Stabilizing high-period orbits in a chaotic system: the diode resonator," Phys. Rev. Lett. **67**, 1953 (1991).

26 V. Petrov, V. Gaspar, J. Masere, and K. Showalter, "Controlling chaos in the belousov-zhabotinsky reaction," Nature **361**, 240 (1993).

27 A. Garfinkel, M. L. Spano, W. L. Ditto, and J. N. Weiss, "Controlling cardiac chaos," Science **257**, 1230 (1992).

28 W. Just, D. Reckwerth, E. Reibold, and H. Benner, "Influence of control loop latency on time-delayed feedback control," Phys. Rev. E **59**, 2826 (1999).

29 P. Hövel and J. Socolar, "Stability domains for time-delay feedback control with latency," Phys. Rev. E **68**, 36206 (2003).

30 D. W. Sukow, M. E. Bleich, D. J. Gauthier, and J. E. S. Socolar, "Controlling chaos in fast dynamical systems: Experimental results and theoretical analysis," Chaos **7**, 560 (1997).

31 J. Farmer, "Chaotic attractors of an infinite-dimensional dynamical system," Physica D **4D**, 366 (1982).

32 G. Mykolaitis, A. Tamasevicius, A. Cenys, S. Bumeliene, A. N. Anagnostopoulos, and N. Kalkan, "Very high and ultrahigh frequency hyperchaotic oscillators with delay line," Chaos, Solitons and Fractals **17**, 343 (2003).

33 J. P. Goedgebuer, L. Larger, and H. Porte, "Optical cryptosystem based on synchronization of hyperchaos generated by a delayed feedback tunable laser diode," Phys. Rev. Lett. **80**, 2249 (1998).

34 K. Ikeda, K. Kondo, and O. Akimoto, "Successive higher-harmonic bifurcations in systems with delayed feedback," Phys. Rev. Lett. **49**, 1467 (1982).

35 K. Myneni, T. A. Barr, N. J. Corron, and S. D. Pethel, "New method for the control of fast chaotic oscillations," Phys. Rev. Lett. **83**, 2175 (1999).

36 N. Corron, B. Hopper, and S. Pethel, "Limiter control of a chaotic RF transistor oscillator," Int. J. Bifurcation and Chaos **13**, 957 (2003).

37 K. Pyragas, "Continuous control of chaos by self-controlling feedback," Phys. Lett. A **170**, 421 (1992).

38 K. Ogata, *Modern Control Engineering, 2nd Ed.* (Prentice-Hall, Englewood Cliffs, NJ, 1990).

39 R. M. Corless, G. H. Gonnet, D. E. G. Hare, D. J. Jeffry, and D. E. Knuth, "On the lambert *W* function," Adv. Comput. Math. **5**, 329 (1996).

40 L. E. El'sgol'ts and S. B. Norkin, *Introduction to the Theory and Application of Differential Equations with Deviating Arguments* (Academic Press, New York, 1973).

41 K. Pyragas and A. Tamasevicius, "Experimental control of chaos by delayed self-controlling feedback," Phys. Lett. A **180**, 99 (1993).

42 D. Gauthier, D. Sukow, H. Concannon, and J. Socolar, "Stabilizing unstable periodic orbits in a fast diode resonator using continuous time-delay autosynchronization," Phys. Rev. E **50**, 2343 (1994).

43 C. von Loewenich, H. Benner, and W. Just, "Experimental relevance of global properties of time-delayed feedback," Phys. Rev. Lett. **93**, 174101 (2004).

44 O. Lüthje, S. Wolff, and G. Pfister, "Control of chaotic taylor-couette flow with time-delayed feedback," Phys. Rev. Lett. **86**, 1745 (2001).

45 R. Dykstra, D. Y. Tang, and N. R. Heckenberg, "Experimental control of single-mode laser chaos by using continuous, time-delayed feedback," Phys. Rev. E **57**, 6596 (1998).

46 H. Benner and W. Just, "Control of chaos by time-delayed feedback in high-power ferromagnetic resonance experiments," J. Kor. Phys. Soc. **40**, 1046 (2002).

47 T. Pierre, G. Bonhomme, and A. Atipo, "Controlling the chaotic regime of nonlinear ionization waves using the time-delay autosynchronization method," Phys. Rev. Lett. **76**, 2290 (1996).

48 E. Gravier, X. Caron, G. Bonhomme, and T. Pierre, "Control of the chaotic regime of nonlinear drift-waves in a magnetized laboratory plasma," Phys. Plasmas **6**, 1670 (1999).

49 C. Beta, M. Bertram, A. S. Mikhailov, H. H. Rotermund, and G. Ertl, "Controlling turbulence in a surface chemical reaction by time-delay autosynchronization," Phys. Rev. E **67**, 046224 (2003).

50 I. Z. Kiss, Z. Kazsu, and V. Gaspar, "Tracking unstable steady states and periodic orbits of oscilllatory and chaotic electrochemical systems using delayed feedback control," Chaos **16**, 033109 (2006).

51 J. Socolar, D. Sukow, and D. Gauthier, "Stabilizing unstable periodic orbits in fast dynamical systems," Phys. Rev. E **50**, 3245 (1994).

52 K. Pyragas, "Control of chaos via extended delay feedback," Phys. Lett. A **206**, 323 (1995).

53 M. E. Bleich and J. E. S. Socolar, "Stability of periodic orbits controlled by time-delay feedback," Phys. Lett. A **210**, 87 (1996).

54 W. Just, T. Bernard, M. Ostheimer, E. Reibold, and H. Benner, "Mechanism of time-delayed feedback control," Phys. Rev. Lett. **78**, 203 (1997).

55 S. Kobayashi, Y. Yamamoto, M. Ito, and T. Kimura, "Direct frequency modulation in algaas semiconductor lasers," IEEE J. Quantum Electron. **18**, 582 (1982).

56 C.-Y. Tsai, C.-H. Chen, T.-L. Sung, C.-Y. Tsai, and J. M. Rorison, "Theoretical modeling of carrier and lattice heating effects for frequency chirping in semiconductor lasers," Appl. Phys. Lett. **74**, 917 (1999).

57 J. N. Blakely, L. Illing, and D. J. Gauthier, "High-speed chaos in an optical feedback

system with flexible timescales," IEEE J. Quantum Electron. **40**, 299 (2004a).

58 W. Michiels, K. Engelborghs, P. Vansevenant, and D. Roose, "Continuous pole placement for delay equations," Automatica **38**, 747 (2002).

59 J. N. Blakely, L. Illing, and D. J. Gauthier, "Controlling fast chaos in delay dynamical systems," Phys. Rev. Lett. **92**, 193901 (2004b).

60 F. O. Ilday, J. Buckley, H. Lim, F. Wise, and W. Clark, "Generation of 50-fs, 5-nJ pulses at 1.03 μm from a wave-breaking-free fiber laser," Opt. Lett. **28**, 1365 (2003).

Index

Titel. Author(s)

ISBN: 3-527-XXXXX-X